Journal of
Materials Chemistry C

Accepted Manuscript

This article can be cited before page numbers have been issued, to do this please use: X. Zhang, S. Bi, J. Zhou, S. You, H. Zhou, Y. Zhang and Z. Tang, *J. Mater. Chem. C*, 2017, DOI: 10.1039/C7TC02646C.

ROYAL SOCIETY OF CHEMISTRY

rsc.li/materials-c

View Article Online
DOI: 10.1039/C7TC02646C

Journal Name

ARTICLE

Temperature-Dependent Charge Transport in Solution-Processed Perovskite Solar Cells with Tunable Trap Concentration and Charge Recombination†

Received 00th January 20xx,
Accepted 00th January 20xx

DOI: 10.1039/x0xx00000x

www.rsc.org/

Xuning Zhang,[a] Shiqing Bi,[b] Jiyu Zhou,[a] Shuai You,[b] Huiqiong Zhou,*[,b] Yuan Zhang,*[,a] and Zhiyong Tang[b]

Here we investigate temperature-dependent charge transport in solution-processed methylammonium lead triiodide ($MAPbI_3$) perovskite thin films with steady-state mobility measurements. Based on the control of thickness (*L*) of $MAPbI_3$ films, one attains a tunability in carrier mobility, trap density and recombination that lead to varying the device characteristics. We find that the increased hole mobility in $MAPbI_3$ with incremental variation on *L* is associated with the reduction in trap concentration and Shockley-Read-Hall (SRH) recombination. By interrogating the ideality factor, we identify that the SRH charge recombination is present in the optimal solar cell. Of interest, the impact of traps on recombination becomes weakened and eventually is overwhelmed by bimolecular recombination with increasing *L*. Photoluminescence decay kinetics reveals that the PL related to surface and bulk recombination is both longer-lived at larger *L*, in line with the results based on electrical analysis. The meliorated transport properties with reduced charge trapping in $MAPbI_3$ films can correlate to the slightly enhanced crystallinity and homogeneity in grain size distribution in thicker films. The combinatorial study evidences that the transport properties alongside traps in $MAPbI_3$ films are tunable simply by the physical parameter of *L*. In the meanwhile, our work points to the necessity to further reduce the trap density so as to boost the photovoltaic performance using perovskite thin films.

Introduction

Hybrid organic-inorganic lead halide perovskites ($MAPbX_3$) have become an intensive research topic because of attractive applications in energy conversion and photonic devices.[1,2,3,4,5,6,7,8,9] $MAPbX_3$ with the ABX_3 structure comprises of an organic cation (A), a metal cation (B), and halide anions (X).[10] To date, state-of-the-art perovskite solar cells using mixed organic cations and halide anions have shown a power conversion efficiency (PCE) exceeding 22%.[11,12] This competitive performance is attributed to the merits of high carrier mobility, large dielectric constant, high degree of crystallinity, and excellent band-gap tunability.[13,14,15,16,17,18] Along with continuous efforts to boosting the device performance, there is growing interest of fundamentally understanding the optoelectronic properties in hybrid perovskites that govern the solar cell characteristics.[12,13,14,15,19,20,21] With transient absorption spectroscopy, intrinsic carrier mobility in $MAPbI_3$ was probed, revealing an extreme shallow trap depth and low trap density.[13] Similar optical measurements indicated that balance between hole and electron mobilities in $MAPbI_3$ after charge dissociation was maintained within a timescale up to microsecond.[22] Aided by first-principle calculation, ionic transport in $MAPbI_3$ was investigated which was identified to be driven by the vacancy in the lattice, showing an activation energy of 0.6 eV.[14] Furthermore, Hall measurements unravelled that the intrinsic carrier mobility in $MAPbI_3$ films was up to 60 cm^2/Vs which led to a very low electron-hole recombination rate.[23]

Although these understandings are insightful, the information extracted from these techniques might not entirely reveal steady-state solar cell operation with a sandwich device architecture. For example, the charge transport direction examined by Hall mobility measurements differs from that in operating solar cells relying on an out-of-plane charge transporting path. To this end, it appears more relevant to explore steady-state transport properties in the same direction with that in solar cells using diode mobility measurements. By doing so, one simultaneously attains the information on diode mobility in the space-charge limited current (SCLC) regime and traps.[24,25] Generally speaking, sufficient carrier mobility with minimized traps is essential to

[a] Heeger Beijing Research and Development Center, School of Chemistry, Beihang University, Beijing 100191, P. R. China.
[b] CAS Key Laboratory of Nanosystem and Hierarchical Fabrication, CAS Center for Excellence in Nanoscience National Center for Nanoscience and Technology, Beijing 100190, P. R. China

†Electronic Supplementary Information (ESI) available: See DOI: 10.1039/x0xx00000x

View Article Online
DOI: 10.1039/C7TC02646C

attain satisfactory device characteristics. When trap-assisted (Shockley-Read-Hall, or SRH) recombination becomes dominate, unfavourable losses of photo-carriers and eventually PCEs may occur.[26,27] To date, the knowledge on how charge trapping affects to the diode transport behavior relevant to solar cell operation and recombination processes in $MAPbX_3$ films yet remains poorly understood.

In this article, based on the control of the perovskite film thickness (*L*), we investigate temperature (*T*)-dependent steady-state charge carrier transport, recombination and traps in methylammonium lead triiodide ($MAPbI_3$) films and correlate these properties to solar cell parameters. We found that the trap concentration and charge recombination are tunable through controlling the *L*, leading to varied device characteristics. The carrier mobility is improved in association with reduced densities of traps when incrementally varying *L*, while surprisingly a reduction of PCE is observed in corresponding solar cells. The melioration of carrier transport and charge trapping with increasing *L* is confirmed by PL decay kinetics and ideality factor (IF) measurements. The results indicates that the decreased in PCE in thick cells may be ascribed to other factors e.g. the limitation of carrier diffusion distance which highlight the necessarily to further increase the carrier mobility. More relevantly, this work points to the significance of reducing trap concentrations so as to approach the potential of hybrid perovskite solar cells.

Results and Discussion

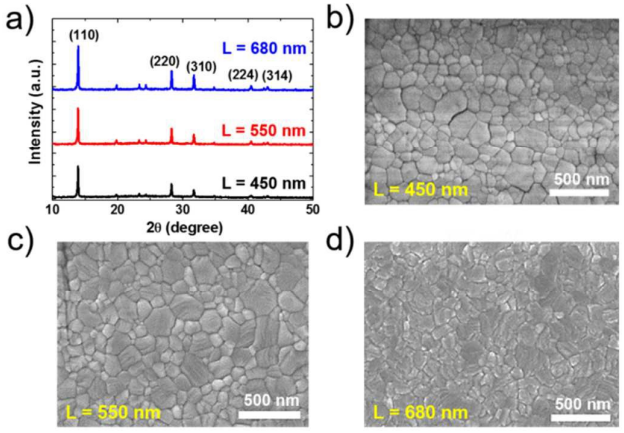

Fig. 1. XRD patterns of $MAPbI_3$ thin films with different *L*. (b)-(d) Top view SEM images of corresponding perovskite thin films.

To understand the morphology changes brought by the variation of *L* in $MAPbI_3$ films, we first measured scanning electron microscopy (SEM) characteristics along with X-ray diffractometry (XRD). As shown in Fig. 1a, the 680 nm film displays a slightly enhanced crystallinity and surface uniformity with dense and flattened structures. Clearly the distribution of grain sizes becomes more homogeneous with the film thickness (see Fig. 1b-1d). This may suggest an improved film-forming quality with possibly reduced grain boundaries when using more concentrated precursor solutions. These morphological and structural merits hint that the corresponding opto-electrical properties may be modified as a function of *L*.

To examine the resultant photovoltaic behavior, we fabricated $MAPbI_3$ solar cells adopting the inverted device architecture (see Fig. 2a) which affords a high reproducibility, ease of characterization and device fabrication, although we acknowledge that this simple structure often yields lower PCEs compared to devices containing multiple interlayers or using mesoporous TiO_2 structure. More importantly, this structure allows for more reproducible diode measurements which are essential for our *T*-dependent analysis. To reduce the complexity of interface effects that could lead to different photophysical processes and surface recombination, [28] additional electron extraction interlayers are avoided in our solar cells except for the necessary $PC_{61}BM$. To attain a meaningful comparison, single-carrier devices (here defined as hole-only device or HO) were fabricated based on the identical $MAPbI_3$ photoactive layers with similar architecture where a polymeric hole extraction interlayer based on P3HT was incorporated beneath the Au contact (see Fig. 2b). As a result, the electron injection can be effectively blocked, leading to so-call HO devices.

Fig. 2c shows representative *J-V* characteristics of $MAPbI_3$ solar cells under AM 1.5 G irradiation (100 mW/cm^2) measured at room temperature (*RT*) in the downward scan (for bias from positive to negative) to avoid the effect of hysteresis. All devices were tested in nitrogen environment without encapsulation. Detailed solar cell parameters are summarized in Table S1 in the Supporting information (SI). Among these cells, we found that the device with *L* = 450 nm yielded a maximal PCE over 12%, in in line with previous results based on single charge extraction interlayers.[29] With enlarging *L* (from 450, 550 to 680 nm), we note that the short-circuit current (J_{sc}, from 17.47, 14.20 to 11.94 mA/cm^2), open-circuit voltage (V_{oc}, from 0.98, 0.92 to 0.88 V) and ultimate PCE all decrease while the fill factor (*FF*, from 0.72, 0.77 to 0.78) exhibits an opposite trend to decrease. Through enlargement of *L,* one expect to obtain a gain in photon-absorption and thus an increased J_{sc}. Counterintuitively, our results suggest that other restraining factors may be responsible for the reduced J_{sc} and V_{oc} in thick devices, which will be discussed in below. The systematically changed solar cell parameters afford a base for investigating the optoelectronic properties of $MAPbI_3$ films at different *L*.

Next, we focus on charge carrier transport in $MAPbI_3$ films using single-carrier devices. As illustrated by the energy diagram in Fig. 2d, with ohmic injection (meaning the energy of valence or conduction band matches the work function of electrodes), the transport in a semiconductor can be divided into three regimes including ohmic current at low bias due to the presence of background carriers, [30] trap-filling current (TFC) at intermediate voltage where injected carriers mainly fill the traps and space-charge limited current (SCLC) where mobile carries dominate the transport. To verify this, we comparatively show *J-V* characteristics (300 K) of HO devices with various *L*. Consistently, we observe three discernible curve slopes at different biases (see lines in Fig. 3a). These

View Article Online
DOI: 10.1039/C7TC02646C

transitions are reproducibly seen in *J-V* curves measured within a wide range of *T* (see Fig. S1, SI). The background carrier density is low in our devices without intentional doping, thus the resulting ohmic behavior occurs within a very small bias regime. Beyond that, the super-linear current rapidly increases with voltage, a fingerprint for TFC.[31] This behavior has also been observed in $MAPbI_3$ single crystals even with an extremely low trap density.[32] With further increasing the bias, the TFC gradually vanishes and the slope becomes less steep, leading to a quadratic voltage dependence indicating the SCLC. In this regime, the hole mobility (μ_p) can be determined by using the well-established Mott-Gurney law.[33] As the P3HT interlayer in HO devices is very thin (~20 nm), the *T*-dependence mainly reflects the situation of the transport through $MAPbI_3$ films.

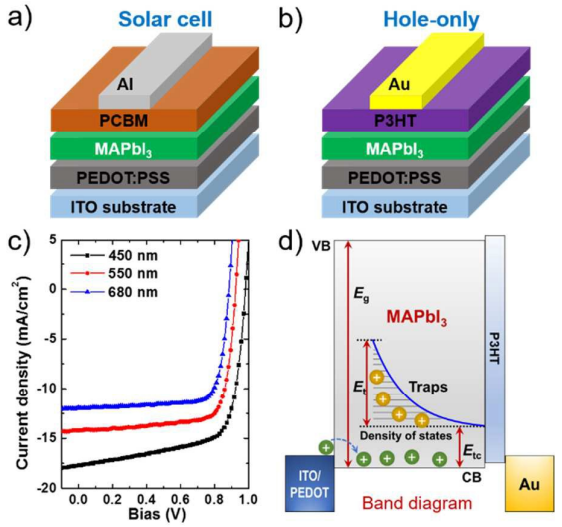

Fig. 2. Device architectures of (a) solar cell and (b) hole-only device used in this study based on methylammonium lead triiodide ($MAPbI_3$) films. (c) Current density versus voltage (*J-V*) characteristics of $MAPbI_3$ solar cells with various film thicknesses (*L*) measured under AM 1.5 G solar irradiation (100 mW/cm^2). (d) Energy diagram for $MAPbI_3$ single-carrier (hole-only) devices. Also included is an illustration of the exponential density of states of traps within the band gap (VB: valence band, CB: conduction, see other abbreviations defined in text).

The impact of traps on the SCLC transport was first addressed by Mark and Helfrich.[34] Generally, in a semiconductor with traps, the current reduces by $(N_t/N)^r$ with N_t denoting the density of trapped carriers, *N* denoting the total carrier density and *r* as a power factor related to the trap distribution. In Fig. 2d, an exponential density of states (DOS) for the traps in $MAPbI_3$ films is illustrated with $N(E) = N_v(c)\exp(-E/E_t)$ where $N(E)$ describes the DOS, $N_v(c)$ is the trap density at the valence band (or conduction band edge), and E_t is the characteristic trap width. The TFC transport is analytically described by the equation in below,[34]

$$J = N_c q\mu \left(\frac{\varepsilon_0\varepsilon_r}{qN_t e^{Etc/Et}}\right)^r \left[\left(\frac{2r+1}{r+1}\right)^{r+1}\left(\frac{r}{r+1}\right)^r\right]\frac{V^{r+1}}{L^{2r+1}} \quad (1)$$

where N_c is the total allowing states, *q* is the elementary charge, μ is the mobility of free carriers, $\varepsilon_0\varepsilon_r$ ($\varepsilon_r = 25$ in our case and ε_0 is the vacuum permittivity) is the dielectric constant of $MAPbI_3$, E_{tc} is the energetic position of the trap center (or trap depth) and E_t is the trap width, and $r = E_t/k_BT$ (see Fig. 2d). As shown by Equation 1, the *r* value can be determined from the slope of *J-V* characteristics in the TFC regime in Fig. 3a. Then the parameter of E_t is extracted from the slope in the plot of *r* vs. *T*.[35] Based on dark transport characteristics of $MAPbI_3$ HO devices (see. Fig. S1, SI), Fig. 3b shows the determined *r* against *T* for various *L*. In The trap width (E_t) was determined by linear fitting to the plot of *r* vs. *T* in the range between 180 – 300 K. We obtained E_t = 68, 64, and 67 meV for *L* = 450, 550 and 680 nm respectively. These values indicate that the trap within the band gap of $MAPbI_3$ films may have a narrow distribution. For comparison, the determined E_t is also lower than that typically found in solution-processed semi-conductive polymers.[36] Interestingly, the trap width hardly varies with *L*, seemingly an intrinsic parameter. It should be mentioned that from our TFC fittings using Equation 1, the parameter of E_{tc} referring to the energetic position of trap center in $MAPbI_3$ (with regard to valence band) is yet undetermined. This is mainly restrained by the unawareness of the mobility of mobile (non-trapped) carriers. Note that previous studies indicate that extremely shallow traps with a depth of ~50 meV could be present in $MAPbI_3$ films based on optical transient techniques.[13]

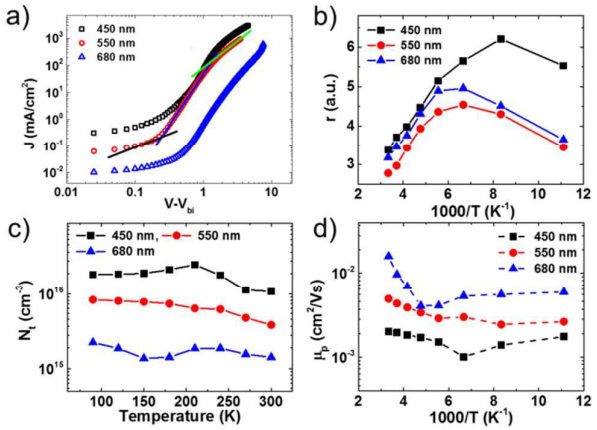

Fig. 3. (a) Comparison of *J-V* characteristics at 300 K for HO devices with different thicknesses in double logarithm scale. Lines in black, blue and green are guide to the eye with slope = 1, ohmic current, slope > 3, TFC, and slope = 2, SCLC. (b) Slope (*r*) of *J-V* characteristics of $MAPbI_3$ HO devices in the TLC regime as a function of temperature (*T*). (c) Trap density N_t, and (d) hole mobility μ_p as a function of *T* determined with hole-only diode measurements on $MAPbI_3$ films in the TLC and SCLC regimes, respectively.

To enable a more quantitative estimation on these traps, we determined the total trap density N_t from the transition voltage for the linear (ohmic) to TFC behaviour (defined as V_{tr}, see Fig. 3a) using the equation in follow.[32]

$$N_t = \frac{2\varepsilon_0\varepsilon_r V_{tr}}{qL^2} \quad (2)$$

Equation 2 was successfully applied to assess the impurities in perovskite single crystals.[32] The determined N_t is plotted as a function of *T* in Fig. 3c for various *L*. At *RT*, we obtained N_t = 1.08×10^{16} cm^{-3}, N_t = 3.8×10^{15} cm^{-3} and N_t = 1.4×10^{15} cm^{-3} for the three devices. These values in $MAPbI_3$ films are

View Article Online
DOI: 10.1039/C7TC02646C

approximately 4 orders higher than that in $MAPbI_3$ single crystals, which can be attributed to larger numbers of structural defects or grain boundaries in solution-processed polycrystalline films.[32] Of note, the trap density decreases with increasing *L* with a weak *T*-dependence, resulting in a negative *T*-coefficient within 210-300 K. This result indicates that more pronounced charge trapping is likely at lower *T*, which is similarly observed in planar diodes based on $MAPbI_3$.[37] Note that within 210-300 K the tetragonal phase should be dominant and phase transition is unlikely in this *T* range.[38,39] In our case, the *T*-dependence for mobility in the tetragonal phase is roughly described by the Arrhenius temperature dependence which has been observed in previous.[40]

Next, we estimate carrier mobility in $MAPbI_3$ in the SCLC regime. The hole mobility was determined by fitting the results in Fig. S1 (SI) to Mott-Gurney law as,

$$J = \frac{9}{8}\varepsilon_0\varepsilon_r\mu_p\frac{(V-V_{bi})^2}{L^3} \quad (3)$$

where μ_p is the hole mobility, V_{bi} is the built-in potential (mainly originating from the difference in anode-cathode work functions). Fig. 3d shows Arrhenius plots of the determined μ_p as a function of *T*. The mobility falls in a range of 10^{-2}-10^{-3} cm^2/Vs with *T* spanning over 200 K. It is noted that two discernible *T*-regimes are observed with distinct *T*-dependencies. In the high temperature regime (210-300 K), the mobility in $MAPbI_3$ single-carrier devices displays a negative *T*-coefficient. This is likely ascribed to the containing ionic transport nature in $MAPbI_3$ films where the ionic conductivity tends to reduce at lower *T*, revealed in a recent study on $MAPbI_3$ field-effect transistors,[41] At lower *T* (< 210 K), the weak *T*-temperature may reflect more intrinsically the electronic conduction in perovskite films. Of note, simply varying *L*, the mobility can be tuned by about 1 order or magnitude. The observed *T*-dependence of hole mobility at higher *T*-regime being inversely proportional to N_t but proportional to *L* is in line with the general trend in the presence of traps.[42]

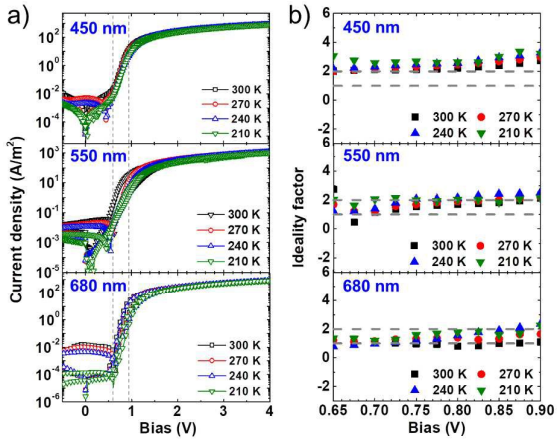

Fig. 4. (a) Dark *J-V* characteristics (in semi-logarithm scale) of $MAPbI_3$ solar cells with various *L* at selected *T*. (b) Ideality factor (IF) determined in the diffusion current regime (within the two dashed vertical lines) of *J-V* characteristics of corresponding solar cells. Dashed horizontal lines in (b) are guide for the eye to indicate IF = 1 and IF = 2, respectively.

With the notion that traps play an important role in charge recombination processes and resulting carrier losses in solar cell operation,[43] a relevant question arises if the identified hole traps can result in trap-assisted (or SRH) charge recombination in $MAPbI_3$ films. By means of examining IF, trap-assisted recombination vs. bimolecular recombination is discernible. Generally, IF = 2 indicates a dominant trap-assisted recombination while IF = 1 suggests the absence of SRH recombination or a dominant bimolecular recombination via non-trapped mobile carriers.[44,45] We investigated IF based on *T*-dependent dark transport in $MAPbI_3$ solar cells with various *L* (see results in Fig. 4a). The current density of all devices exhibits relatively weak *T*-dependence with negative *T*-coefficient, consistent to the observation in HO devices. The pronounced rectification is due to exclusive charge injection in solar cells. According to Schottky equations, the value of IF can be determined from in the diffusion current regime (in our case from 0.6 V to 0.9 V) of *J-V* curves in Fig. 4a by using the relation as,[46]

$$IF = \left(\frac{k_BT}{q}\frac{\partial \ln J}{\partial V}\right)^{-1} \quad (4)$$

where k_B is the Boltzmann constant. Fig. 4b shows the determined IF at different *T* for $MAPbI_3$ solar cells. Near *RT*, it is obvious that the IF of the optimal cell (*L* = 450 nm) roughly hits 2 (see dashed line) while that of the 550 nm device decreases to values between 1.5 and 2. When enlarging *L* to 680 nm, the IF decreases more, approaching unity. In all cases, the IF is slightly increased at lower *T*, consistent to previous observation.[45,47] Of importance, the IF results provide evidence that trap-assisted charge recombination is still present in the optimal device which seems to correlate to the observed TFC behavior in HO devices. The SRH recombination attenuates with enlarging *L*, revealed by the decreased IF approaching unity. This result agrees with the reduced in thicker films, suggesting that in the 680 nm cell, trap-assisted SRH recombination may be less significant and instead bimolecular recombination via mobile carriers becomes more pronounced. Although the value of IF only qualitatively manifests the recombination type rather than the strength, the reduced SRH recombination with increasing *L* is fully consistent to the result on traps. At this moment, we cannot discern whether the SRH recombination in solution-processed $MAPbI_3$ solar cells is radiative or non-radiative.

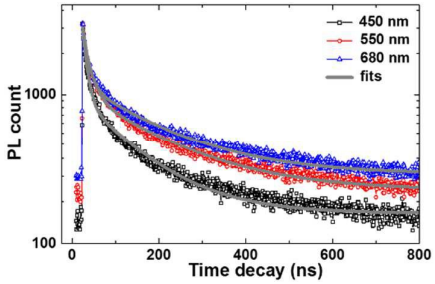

Fig. 5. Photoluminescence decay kinetics (open symbols) of $MAPbI_3$ thin films with different *L* probed at 778 nm. Lines are fittings using a bi-exponential decay model.

View Article Online
DOI: 10.1039/C7TC02646C

To shed more light on the impact of *L* on photophysical processes in $MAPbI_3$ films, at last we performed photo-luminescent (PL) decay kinetics. The influence of *L* on the recombination related to surface and bulk properties in $MAPbI_3$ films is further revealed. Steady-state PL spectra of $MAPbI_3$ films are provided in Fig. S2, showing red-shifts as a function of *L*. This is consistent to the observation of the enhanced homogeneity in grain size distribution with possibly less grain boundaries in the 680 nm film revealed by SEM (Fig. 1).[48] Fig. 5 shows decays of the according PL which are characteristic of superposition of a fast (τ_1) and a slow decay (τ_2) dynamics, indicating the bi-exponential decay process. The two temporal scales can be assigned to trap states related to the surface condition (fast) and bulk transport properties with fewer trap density (slow), respectively.[49, 50] Based on the fittings with the bi-exponential decay model (see fitting parameters in Table S2, SI), we found that both decays become longer-lived with increasing *L*, e.g. τ_1 is increased from 44.2 ns to 55 ns and τ_2 is increased from 397 ns to 445 ns with *L* increased from 450 to 680 nm. The longer PL lifetime is explained by the reduced influence of charge trapping and enhanced transporting capability in bulk. This agrees with the enhanced carrier mobility with fewer traps at larger *L*. Furthermore, the percentage of the secondary longer-lived decay component increases with *L*, in line with the enhanced bulk transport properties at lower N_t. The PL results along with electrical measurements reveal that charge transport and optical properties in $MAPbI_3$ are highly tunable via the film thickness. In additional, the mitigated surface charge recombination revealed by PL decay kinetics hints that the surface traps density is likely to decrease with increasing *L* which could be mainly responsible for the reduction in the total amount of traps shown in Fig. 3c.

It is not so surprising that the charge transport properties and traps densities are changed with variation on *L*. While it seems counterintuitive that although enhanced carrier mobility with reduced trap density is observed at larger *L*, the according photovoltaic performance is oppositely decreased, mainly suffering from reduced J_{sc} and V_{oc}. In thicker solar cells, the more severe V_{oc} losses could be ascribed to the increased recombination current with the possible enhancement of absorption and resultant increase in photo-carriers at larger *L*. In this regard, an enlargement of J_{cs} is expected which however is opposite our observation. Another likely explanation may be related to the change of built-in potential (V_{bi}) with enlargement *L*. As V_{bi} provides a driving force for charge separation in solar cells, the reduced V_{bi} in thicker devices may cause more substantial losses of photo-carriers such that the J_{sc} is lowered. Here we emphasize that a full correlation of transport properties with according solar cell parameters may be still of challenge. Concerning the complexity of charge generation/extraction processes, simply by enlarging *L* to gain the photocurrent seems to be unrealistic as other factors such as optical effects may play a role. More importantly, the influences of traps on charge transport and recombination in the optimal devices point to the necessity to further reduce the density of traps e.g. through optimizing the crystallinity and grain sizes in $MAPbX_3$ films.

Conclusions

To summarize, we present a comprehensive investigation to understand charge transport, recombination and photoluminescence properties in solution-processed $MAPbI_3$ thin films and related devices. The solar cell parameters, hole mobility and trap concentration are highly tunable via the $MAPbI_3$ film thickness. In a wide range of temperature (90 K - 300 K), the hole transport in $MAPbI_3$ exhibits evident TFC behavior. The total trap density is estimated to be around 10^{15} - 10^{16} cm^{-3} with the trap width of 64 meV. We find that the hole mobility is enhanced with increasing *L*, in association with reduced charge trapping and longer-lived PL. In the optimal solar cell, trap-assisted recombination is still identified and it becomes less pronounced with enlargement of *L*, leading to a dominant bimolecular recombination. The improved opto-electrical properties can correlate to the slightly enhanced crystallinity and homogeneity in the distribution of grain sizes in thicker films. The combinatorial results suggest that a further boost of PCEs could be benefited from improved control on the traps in $MAPbI_3$. This work assists to fundamentally understand opto-electrical properties that govern the device behavior in solution-processed $MAPbI_3$ solar cells.

Experimental

Material: PbI_2 (99.999%, Sigma Aldrich) and CH_3NH_3I ((Dyesol Ltd, Australia, purity scale: 99.8 %, Dyesol) were used as received. PEDOT:PSS (AL 4083 Clevios) and $PC_{61}BM$ were purchased from H.C. Starck GmbH and Lumtec (Taiwan), respectively.

Device Fabrication: Glass substrates (size = 1.5 cm × 1.5 cm) pre-patterned with the ITO (indium-tin-oxide) anode were sequentially cleaned with detergent solution, acetone, and isopropanol in a sonication bath. For the hole transport layer, commercial PEDOT:PSS (Al 4083) solution was spun-cast on pre-cleaned and UV-zone treated ITO/glass substrates in air at 2000 rpm for 40 s. The solutions of $CH_3NH_3PbI_3$ in N,N-diethylformamide (DMF, Sigma-Aldrich) (concentration: 45 wt%, 50 wt% and 55 wt%) were prepared by mixing PbI_2 and CH_3NH_3I in a molar ratio of 1:1 in DMF. The triiodide perovskite layers were obtained as follows: 35 µL of $CH_3NH_3PbI_3$ solution was dropped onto the ITO substrate and then were spun-coat at 6000 rpm. At around 6 s before ending, 105 µl of chlorobenzene was dropped on the perovskite film to accelerate the crystallization. After that a spin-dying at the same rpm was applied for 30 s. The cast films were transferred on a hotplate and annealed at 100 °C for 10 min. For the electron transporting layer, 20 mg of $PC_{61}BM$ (Lumtec, Taiwan) was first solubilized in 1 mL chlorobenzene. Then 20 µL of $PC_{61}BM$ solution was spun-coat on the perovskite active layer with a spin-rate of 2000 rpm for 40 s. For the hole transporting layer in single carrier devices, region-regular P3HT (Lumtec, Taiwan) was deposited atop the $MAPbI_3$ layer from the chlorobenzene solution in a concentration of 10 mg/mL, leading

DOI: 10.1039/C7TC02646C

to a film thickness of ~20 nm. Finally, 100 nm of aluminium (for solar cells) or Au (for single carrier devices) top electrodes were thermally evaporated atop the $PC_{61}BM$ layer (solar cell) or P3HT layer (single carrier device) under vacuum (< 10^{-6} mbar). The finished devices were kept in a nitrogen-purged glove box before testing.

Characterization: The thicknesses of perovskite films were determined by a profilometer (KLA Tencor D-120). The morphology was characterized by a scanning electron microscope (S4800, Hitachi, Japan). Crystallinity was examined by using a X-ray diffractometer (Philips X'Pert) equipped with Cu Kα radiation (λ = 1.5419 Å). Transmittance and absorbance spectra were obtained with a UV-vis spectrometer (PE Lambda 650/850/950 UV-vis spectrophotometer). *J-V* characteristics of solar cells were recorded by a Keithley 2400 SourceMeter under AM 1.5 G illumination (100 mW/cm^2) provided by an Oriel solar simulator. The incident light intensity was calibrated with a certified silicon photodiode (Peccell Technologies). Steady-state PL spectra were measured by a HORIBA Fluorolog-III spectrofluoroemeter. The PL lifetime was probed by a customized spectrometer system (Fluorolog-III, HORIBA Jobin-Yvon Inc) equipped with a diode laser (λ = 460 nm) for excitation under an operation voltage at 950 V for the detector with peak preset = 3000 counts. Single carrier devices were characterized in a vacuum probe station (LakeShore Inc.) using a Keithley 4200-SCS semiconductor parameter analyser. Low *T* was attained by liquid nitrogen with *T* adjusted by a LakeShore temperature controller.

Acknowledgements

Y. Z. thanks for the support of the National Natural Science Foundation of China (No. 21674006) and the Young Talents Thousand Program and H.Z. acknowledges the support from the Chinese Academy of Sciences (100 Top Young Scientists Program and QYZDB-SSW-SLH033).

Notes and references

1 H. Zhou, Q. Chen, G. Li, S. Luo, T. B. Song, H. S. Duan, Z. Hong, J. You, Y. Liu, and Y. Yang, *Science,* 2014, **345**, 542.
2 J. Burschka, N. Pellet, S. J. Moon, R. Humphry-Baker, P. Gao, M. K. Nazeeruddin, and M. Grätzel, *Nature,* 2013, **499**, 316.
3 A. Kojima, K. Teshima, Y. Shirai, and T. Miyasaka, *J. Am. Chem. Soc.,* 2009, **131**, 6050.
4 S. D. Stranks, G. E. Eperon, G. Grancini, C. Menelaou, M. J. P. Alcocer, T. Leijtens, L. M. Herz, A. Petrozza, and H. J. Snaith, *Science,* 2013, **342**, 341.
5 N. J. Jeon, J. H. Noh, Y. C. Kim, W. S. Yang, S. Ryu, S. and I. Seok, *Nat. Mater.,* 2014, **13**, 897.
6 M. A. Green, A. Ho-Baillie, and H. J. Snaith, *Nat. Photonics.,* 2014**, 8**, 506.
7 Y. H. Kim, H. Cho, J. H. Heo, T. S. Kim, N. Myoung, C. L. Lee, S. H. Im, and T. W. Lee, *Adv. Mater.,* 2015, **27**, 1248.
8 G. D. Niu, X. D. Guo, and L. D. Wang, *J. Mater. Chem. A,* 2015, **3**, 8970.
9 T. Baikie, Y. N. Fang, J. M. Kadro, M. Schreyer, F. X. Wei, S. G. Mhaisalkar, M. Graetzel, and T. J. White, *J. Mater. Chem. A,* 2013, **1**, 5628.
10 G. E. Eperon, S. D. Stranks, C. Menelaou, M. B. Johnston, L. M. Herz, and H. J. Snaith, *Energy Environ. Sci.,* 2014, **7**, 982.
11 X. Li, D. Bi, C. Yi, J.-D. Décoppet, J. Luo, S. M. Zakeeruddin, A. Hagfeldt, and M. Grätzel, *Science,* 2016, DOI: 10.1126/science.aaf8060.
12 W. S. Yang, J. H. Noh, N. J. Jeon, Y. C. Kim, S. Ryu, J. Seo, and S. I. Seok, *Science,* 2015, **348**, 1234.
13 H. Oga, A. Saeki, Y. Ogomi, S. Hayase, and S. Seki, *J. Am. Chem. Soc.,* 2014, **136**, 13818.
14 C. Eames, J. M. Frost, P. R. Barnes, B. C. O'Regan, A. Walsh, and M. S. Islam, *Nat. Commun.,* 2015, **6**, 7497.
15 S. Meloni, T. Moehl, W. Tress, M. Franckevicius, M. Saliba, Y. H. Lee, P. Gao, M. K. Nazeeruddin, S. M. Zakeeruddin, U. Rothlisberger, and M. Graetzel, *Nat. Commun.,* 2016, **7**, 10334.
16 E. L. Unger, E. T. Hoke, C. D. Bailie, W. H. Nguyen, A. R. Bowring, T. Heumüller, M. G. Christoforo, and M. D. McGehee, *Energy Environ. Sci.,* 2014, **7**, 3690.
17 H. S. Kim, I. Mora-Sero, V. Gonzalez-Pedro, F. Fabregat-Santiago, E. J. Juarez-Perez, N. G. Park, and J. Bisquert, *Nat. Commun.,* 2013, **4**, 2242.
18 K. Sveinbjörnsson, X. Zhang, M, Pazoki, A. Hagfeldt, G. Boschloo, and E. M. J. Johansson, *J. Phys. Chem. Lett.,* 2015**, 6**, 4259.
19 E. Lafalce, C. Zhang, X. J. Liu, and Z. V. Vardeny, *ACS Appl. Mater. Interfaces.,* 2016, **8**, 35447.
20 C. Wehrenfennig , G. E. Eperon , M. B. Johnston , H. J. Snaith, and L. M. Herz. *Adv. Mater.* 2014, **26**, 1584.

View Article Online
DOI: 10.1039/C7TC02646C

21 A. Filippetti, A. Mattoni, C. Caddeo, M. I. Sabaa and P. Delugas. *Phys. Chem. Chem. Phys.,* 2016, **18**, 15352.

22 C. S. Ponseca, T. J. Savenije, M. Abdellah, K. Zheng, A. Yartsev, T. R. Pascher, T. Harlang, P. Chabera, T. Pullerits, and A. Stepanov, *J. Am. Chem. Soc.,* 2014, **136**, 5189.

23 Y. Chen, H. Yi, X. Wu, R. Haroldson, Y. Gartstein, Y. Rodionov, K. Tikhonov, A. Zakhidov, X.-Y. Zhu, and V. Podzorov, *Nat. Commun.,* 2016, **7**, 12253.

24 E. J. Yoo, M. Lyu, J. H. Yun, C. Kang, Y. J. Choi, and L. Wang, *Adv. Mater.,* 2015, **27**, 6170.

25 P. Qin, H. Kast, M. K. Nazeeruddin, S. M. Zakeeruddin, A. Mishra, P. Bäuerle, and M. Grätzel, *Energy Environ. Sci.,* 2014, **7**, 2981.

26 M. Mandoc, F. Kooistra, J. C. Hummelen, B. De Boer, and P. W. W. M. Blom, *Appl. Phys. Lett.,* 2007, **91**, 263505.

27 T. Kirchartz, B. E. Pieters, J. Kirkpatrick, U. Rau, and J. Nelson, *Phys. Rev. B,* 2011, **83**, 115209.

28 C. S. Ponseca Jr., E. M. Hutter, P. Piatkowski, B. Cohen, T. Pascher, A. Douhal, A. Yartsev, V. Sundström, and T. J. Savenije. *J. Am. Chem. Soc.,* 2015, **137**, 16043.

29 M. Xiao, F. Huang, W. Huang, Y. Dkhissi, Y. Zhu, J. Etheridge, A. Gray-Weale, U. Bach, Y.-B. Cheng, and L. Spiccia. *Angew. Chem. Int. Ed.* 2014, **53**, 9898.

30 S. Berleb A. G. Mückl, W. Brütting, and M. Schwoerer, *Synth. Met.,* 2000, **111**, 341.

31 M. A. Lampert, *Phys. Rev.,* 1956, **103**, 1648.

32 D. Shi, V. Adinolfi, R. Comin, M. Yuan, E. Alarousu, A. Buin, Y. Chen, S. Hoogland, A. Rothenberger, K. Katsiev, Y. Losovyj, X. Zhang, P. A. Dowben, O. F. Mohammed, E. H. Sargent, and O. M. Bakr, *Science,* 2015, **347**, 519.

33 N. F. Mott, R. W. Gurney, *Electronic Processes in Ionic Crystals,* 1964, 2nd ed. Dover, New York.

34 P. Mark, W. Helfrich, *J. Appl. Phys.* 1962*,* **33**, 205.

35 K. K. C.; Wang, W. H, *Physics Bulletin*, 1981, **32,** 235.

36 B. Li, J. Chen, D. Yang, and D. Ma, *Semicond. Sci. Tech.* 2011, **26**, 115006.

37 Y. Yuan, T. Li, Q. Wang, J. Xing, A. Gruverman, and J. Huang, *Sci. Adv.,* 2017, **3**, e1602164.

38 H. H. Fang, R. Raissa, M. Abdu-Aguye, S. Adjokatse, G. R. Blake, J. Even, and M. A. Loi, *Adv. Funct. Mater.,* 2015, **25**, 2378.

39 C. C. Stoumpos, C. D. Malliakas, and M. G. Kanatzidis. *Inorg. Chem.* 2013, **52**, 9019.

40 A. Baumann, S. Väth, P. Rieder, M. C. Heiber, K. Tvingstedt, and V. Dyakonov, *J. Phys. Chem. Lett.,* 2015, **6**, 2350.

41 S. P. Senanayak, B. Yang, T. H. Thomas, N. Giesbrecht, W. Huang, E. Gann, B. Nair, K. Goedel, S. Guha, X. Moya, C. R. McNeill, P. Docampo, A. Sadhanala, R. H. Friend, H. Sirringhaus, *Sci. Adv.*, 2017, **3**, e1601935.

42 M. Mandoc, B. de Boer, G. Paasch, P. Blom, *Phys. Rev. B,* 2007, **75**, 193202.

43 Y. Zhao, and K. Zhu, *J. Phys. Chem. Lett.,* 2013, **4**, 2880.

44 G. Wetzelaer, M. Kuik, L. M. Lenes, and P. Blom, *Appl. Phys. Lett.,* 2011, **99**, 153506.

45 G. J. A. Wetzelaer, N. J Van der Kaap, L. Koster, and P. W. M. Blom, *Adv. Energy Mater.,* 2013**, 3**, 1130.

46 G. J. A. H. Wetzelaer, M. Scheepers, A. M. Sempere, C. Momblona, J. Avila, H. J. Bolink, *Adv. Mater.*, 2015, **27**, 1837.

47 G. Wetzelaer, M. Kuik, H. Nicolai, P. Blom, *Phys. Rev. B,* 2011, **83**, 165204.

48 D. Li, G. Wang, H.-C. Cheng, C.-Y. Chen, H. Wu, Y. Liu, Y. Huang, and X. Duan, *Nat. Commun.,* 2017, **7**, 11330.

49 Y. Yamada, T. Nakamura, M. Endo, A. Wakamiya, and Y. Kanemitsu, *J. Am. Chem. Soc.,* 2014, **136**, 11610.

50 Y. Xing, Y. C. Sun, H.-L. Yip, G. C. Bazan, F. Huang, and Y. Cao, *Nano Energy,* 2016, **26**, 7.

View Article Online
DOI: 10.1039/C7TC02646C

Table of Contents

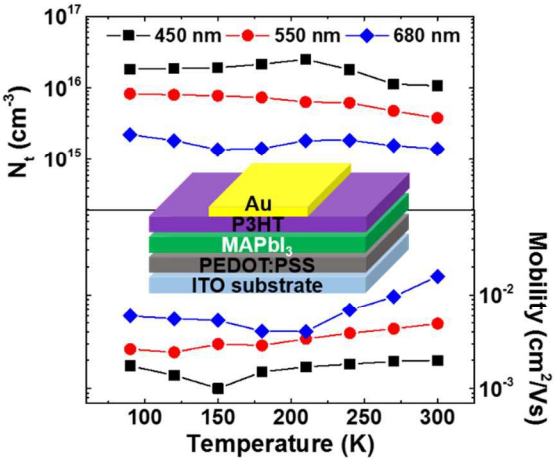

Charge transport, traps and charge recombination in solution-processed methylammonium triiodide halide ($MAPbI_3$) perovskite films are investigated via the control of $MAPbI_3$ film thickness (*L*). Improvements of hole mobility along with reduction in trap density and Shockley-Read-Hall recombination are observed with incremental variation of *L*, leading to a modulation of device parameters in $MAPbI_3$ solar cells.